Guided ion beam and theoretical study of the reactions of Hf^+ with H_2, D_2, and HD

Christopher S. Hinton and P. B. Armentrout[a)]
Department of Chemistry, University of Utah, 315 South 1400 East, Room 2020, Salt Lake City, Utah 84112, USA

(Received 3 June 2010; accepted 4 August 2010; published online 24 September 2010)

The kinetic energy dependences of reactions of the third-row transition metal cation Hf^+ with H_2, D_2, and HD were determined using a guided ion beam tandem mass spectrometer. A flow tube ion source produces Hf^+ in its ^2D ($6s^25d^1$) electronic ground state level. Corresponding state-specific reaction cross sections are obtained. The kinetic energy dependences of the cross sections for the endothermic formation of HfH^+ and HfD^+ are analyzed to give a 0 K bond dissociation energy of $D_0(Hf^+-H)=2.11\pm0.08$ eV. Quantum chemical calculations at several levels of theory performed here generally overestimate the experimental bond energy but results obtained using the Becke-half-and-half-LYP functional show good agreement. Theory also provides the electronic structures of these species and the reactive potential energy surfaces. Results from the reactions with HD provide insight into the reaction mechanisms and indicates that Hf^+ reacts via a statistical mechanism. We also compare this third-row transition metal system with the first-row and second-row congeners, Ti^+ and Zr^+, and find that Hf^+ has a weaker M^+-H bond. As most third-row transition metal hydride cation bonds exceed their lighter congeners, this trend is unusual but can be understood using promotion energy arguments. © *2010 American Institute of Physics*. [doi:10.1063/1.3482663]

I. INTRODUCTION

Insight into the activation of covalent bonds, important processes in many homogeneous and heterogeneous catalytic processes,[1,2] can be obtained in many ways. Among the simplest, and therefore potentially among the most valuable because it can be studied in detail both experimentally and theoretically, is the activation of dihydrogen at single metal centers. The periodic trends in this chemistry are particularly interesting[3,4] and there are now numerous experimental studies of the reactions of the ions of atomic first-row transition metals,[5–16] second-row transition metals,[10,15,17–19] third-row transition metals,[17,20–23] and other metals[24–28] with dihydrogen, reaction (1), and its isotopic analogues.

$$M^+ + H_2 \rightarrow MH^+ + H. \quad (1)$$

In addition to the kinetics and dynamics of this reaction, the guided ion beam methods used in our laboratory can also measure the bond dissociation energy (BDE) of M^+-H by analysis of the kinetic energy dependence of reaction (1).[29–31] Such thermochemistry is of obvious fundamental interest and has implications for understanding a variety of catalytic reactions involving transition metal systems.[1,2]

In an ongoing systematic study of reaction (1) for the third-row transition metal cations, we have previously studied La^+,[17] Ta^+,[20] W^+,[20] Re^+,[22] Ir^+,[23] Pt^+,[21] and Lu^+ (Ref. 17) using guided ion beam tandem mass spectrometry. Previous theoretical studies include all of the third-row transition metal hydride cations.[32–39] We continue these studies here by reporting absolute cross sections as a function of kinetic energy for reactions of H_2, HD, and D_2 with Hf^+ and analyze them to acquire $D_0(Hf^+-H)$. Detailed theoretical calculations on the HfH^+ and HfH_2^+ species were performed to assign electronic structures and explore possible mechanisms for these reactions. Experimental branching ratios for reaction with HD also provide mechanistic insight, which is compared with results for the lighter group IV congeners, Ti^+ and Zr^+.[16,19] Little information exists in the literature on hafnium hydride. Previous work has detected HfH^+ formation by fluorescence spectroscopy,[40] and this species is found to be the dominant product formed in the reaction of Hf^+ with methane at elevated collision energies.[41] In that study, it was found that Hf^+ was relatively unreactive compared to most third-row transition metal cations, a result attributed to the doubly occupied 6*s* orbital of its ^2D ground state.

II. EXPERIMENTAL SECTION

A. General

The guided ion beam tandem mass spectrometer on which these experiments were performed has been described in detail previously.[42] Briefly, atomic metal ions are generated in a direct current discharge flow tube (DC/FT) source described below,[43] extracted from the source, accelerated, and focused into a magnetic sector momentum analyzer for mass selection of primary ions. The mass-selected ions are decelerated to a desired kinetic energy and focused into an octopole ion beam guide that uses radio-frequency electric fields to trap the ions in the radial direction and ensure complete collection of reactant and product ions.[44,45] The octopole passes through a static gas cell with an effective length

a)Electronic mail: armentrout@chem.utah.edu.

TABLE I. Electronic states and populations of Hf cations.

State	Configuration	Energy (eV)[a]
^{2}D	$6s^25d^1$	0.227
^{4}F	$6s^15d^2$	0.790
^{4}P	$6s^15d^2$	1.617
^{2}F	$6s^15d^2$	1.710
^{2}D	$6s^15d^2$	2.004
^{2}P	$6s^15d^2$	2.104
^{2}G	$6s^15d^2$	2.173
^{4}F	$5d^3$	2.661
^{2}G	$5d^3$	3.454

[a]Energies are the average of all spin-orbit levels taken from Ref. 54 relative to the $^2D_{3/2}$ ground state level.

of 8.26 cm that contains the reaction partner (here, H_2, HD, or D_2) at a low pressure (usually less than ~0.3 mTorr) so that multiple ion-molecule collisions are improbable. All products reported here result from single bimolecular encounters, as verified by pressure dependence studies. The unreacted parent and product ions are confined radially in the guide until they drift to the end of the octopole where they are extracted, focused, and passed through a quadrupole mass filter for mass analysis of products. Ions are subsequently detected with a secondary electron scintillation ion detector[46] using standard pulse counting techniques. Reaction cross sections are calculated from product ion intensities relative to reactant ion intensities after correcting for background signals.[47] Uncertainties in absolute cross sections are estimated to be ±20%.

The kinetic energy of the ions is varied in the laboratory frame by scanning the dc bias on the octopole rods with respect to the potential of the ion source region. Laboratory (lab) ion energies are converted to energies in the center-of-mass frame (CM) by using the formula $E_{CM}=E_{lab}m/(m+M)$, where m and M are the neutral and ionic reactant masses, respectively. Two effects broaden the cross section data: the kinetic energy distribution of the reactant ion and the thermal motion of the neutral reactant gas (Doppler broadening).[48] The absolute zero and the full width at half maximum (FWHM) of the kinetic energy distribution of the reactant ions are determined using the octopole beam guide as a retarding potential analyzer, as described previously.[47] The distributions of ion energies, which are independent of energy, are nearly Gaussian and have a typical FWHM of 0.4–0.9 eV (lab) in these studies. These values are somewhat larger than is usual for this instrument in part because of the extremely wide energy range needed in these studies (lab energies from 0 to 800 eV). This requires different focusing of the ion beam than is optimal for determining the zero of energy and energy distributions. Uncertainties in the absolute zero of the energy scale are ±0.1 eV (lab).

B. Ion source

Hf^+ ions are produced in a DC/FT source, consisting of a cathode held at a high negative voltage (1.1–1.5 kV) over which a flow of approximately 90% He and 10% Ar passes at a total pressure of 0.3–0.5 Torr. The dc-discharge ionizes Ar and then accelerates these ions into the cathode made of either tantalum or iron with a cavity containing hafnium metal. As the ions are swept down the 1 m flow tube, they undergo ~10^5 thermalizing collisions with He and Ar. No evidence for low-lying excited states of the metal ions (such as cross section features having lower energy thresholds) within about 1% sensitivity is observed under these flow conditions either in this work or in previous studies of Hf^+.[41,49] When compared to a surface ionization source, the DC/FT source has been found to generate Sc^+,[50] Fe^+,[51] Co^+,[52] Ni^+,[53] Ru^+,[18] Rh^+,[18] and Pd^+ (Ref. 18) ions with an average electronic temperature of 700 ± 400 K, and Y^+, Zr^+, Nb^+, and Mo^+ ions with an average electronic temperature of 300 ± 100 K.[19] The various low-lying states of Hf^+ are listed in Table I.[54] Even at the maximum electronic temperature of 1100 K, only the lowest energy spin-orbit level ($^2D_{3/2}$) of Hf^+ is populated to any appreciable degree (96.3%) with the $^2D_{5/2}$ level at 0.378 eV having 2.6% of the population. Conservatively, the average electronic energy, E_{el}, at a temperature of 700 ± 400 K for Hf^+ is 0.006+0.010/−0.006 eV.

C. Data analysis

The cross sections of endothermic reactions are modeled using Eq. (2).[29–31,55–58]

$$\sigma(E) = \sigma_0 \sum_i g_i(E + E_i + E_{rot} - E_0)^n/E, \quad (2)$$

where σ_0 is an energy-independent scaling factor, E is the relative kinetic energy of the reactants, n is an adjustable parameter that characterizes the energy dependence of the process, E_{rot} is the rotational energy of the diatomic reactant (=k_BT at 300 K=0.026 eV), and E_0 is the 0 K threshold for reaction of electronic, vibrational, and rotational ground state reactants. The model involves an explicit sum of the contributions of individual electronic states of the Hf^+ reactant, denoted by i, having energies E_i and populations g_i. Before comparison with the experimental data, Eq. (2) is convoluted with the kinetic energy distributions of the reactant ions and neutral reactants at 300 K. The σ_0, n, and E_0 parameters are then optimized using a nonlinear least-squares analysis to give the best reproduction of the data. Error limits for E_0 are calculated from the range of threshold values for different data sets over a range of acceptable n values combined with the absolute errors in the kinetic energy scale and internal energies of reactant ions.

At energies above $D_0(H_2)$ and $D_0(D_2)$, the analyses include a model for this subsequent dissociation, as outlined in detail elsewhere.[59] This high energy model requires two parameters: E_D fixes the onset for HfH^+ (HfD^+) dissociation and the exponent p determines the energy dependence, similar to n in Eq. (2). For the results shown below, E_D is fixed near the H_2 (D_2) bond energy and the optimum value of p was found to be 2.0.

III. EXPERIMENTAL RESULTS

A. Reactions with H_2 and D_2

Figures 1 and 2 show cross sections as a function of kinetic energy for the bimolecular reaction of H_2 and D_2 with

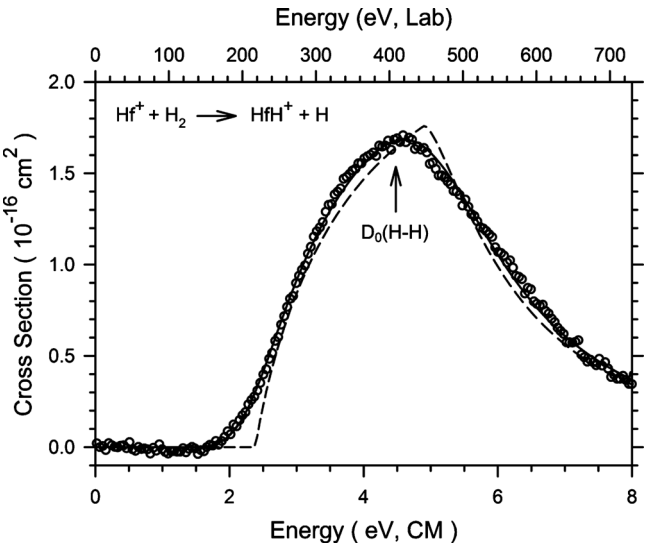

FIG. 1. Cross sections for the reaction of Hf^+ (^2D) with H_2 as a function of kinetic energy in the center-of-mass frame (lower axis) and laboratory frame (upper axis). The best fit to the data using Eq. (2) with parameters of Table II is shown as a dashed line. The solid line shows this model convoluted over the kinetic and internal energy distributions of the reactant neutral and ion. The arrow indicates $D_0(H-H)$ at 4.478 eV.

Hf^+ produced in the DC/FT source. Reaction (1) and its deuterated analogue are the only processes observed. Results for the reaction $Hf^+ + D_2$ are somewhat easier to acquire because the heavier isotope reduces mass overlap between the product ion and the much more intense primary ion, thereby allowing intensities of the product ion to be measured more accurately over a larger dynamic range. However, the same mass resolution conditions were used to collect data for the H_2, D_2, and HD systems here. The absolute magnitudes of the $Hf^+ + H_2$ and $Hf^+ + D_2$ reaction cross sections differ by about 25%, comparable to the estimated 20% experimental

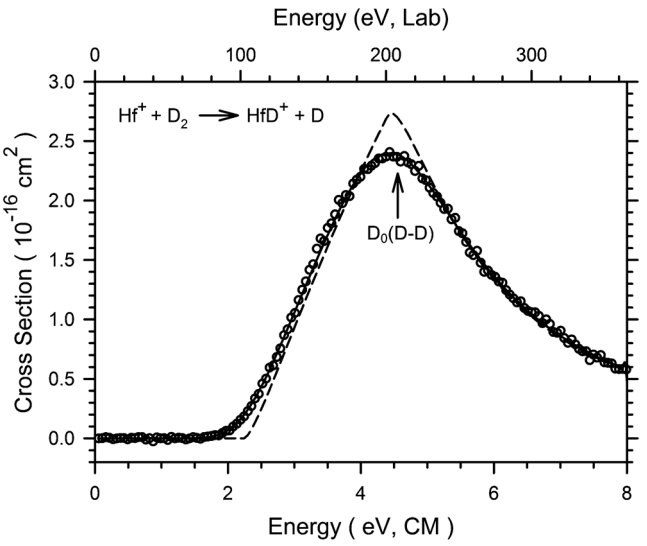

FIG. 2. Cross sections for the reaction of Hf^+ (^2D) with D_2 as a function of kinetic energy in the center-of-mass frame (lower axis) and laboratory frame (upper axis). The best fit to the data using Eq. (2) with parameters of Table II is shown as a dashed line. The solid line shows this model convoluted over the kinetic and internal energy distributions of the reactant neutral and ion. The arrow indicates $D_0(D-D)$ at 4.556 eV.

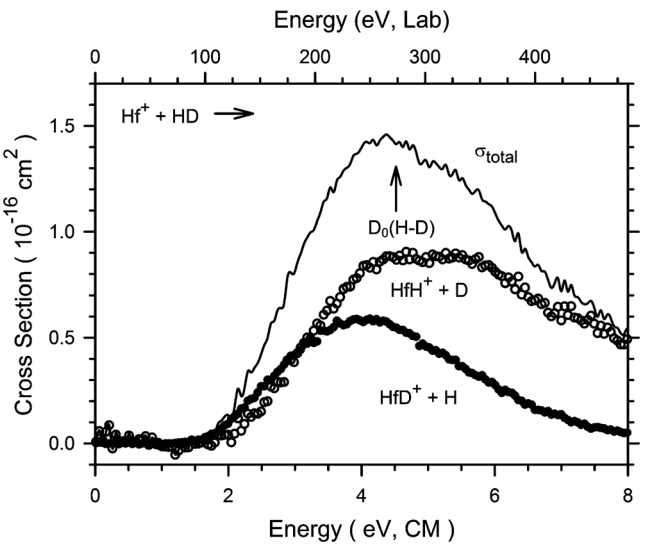

FIG. 3. Cross sections for the reaction of Hf^+ (^2D) with HD as a function of kinetic energy in the center-of-mass frame (lower axis) and laboratory frame (upper axis). The arrow indicates $D_0(H-D)$ at 4.514 eV.

uncertainty. The energy dependences of the cross sections for the two systems are quite similar when plotted on the center-of-mass energy scale.

The cross sections rise from apparent thresholds near 1.7 eV and reach maxima near the dissociation energy of H_2, $D_0(H_2)=4.478$ eV, or D_2, $D_0(D_2)=4.556$ eV.[60] At higher energies, the HfH^+ (HfD^+) products can be formed with internal energies in excess of the BDE, such that these products begin to dissociate in the overall reaction (3)

$$Hf^+ + H_2(D_2) \rightarrow HfH^+(HfD^+) + H(D) \rightarrow Hf^+ + 2H(D). \quad (3)$$

The observation that the experimental cross sections reach maxima very close to the H_2 (D_2) bond energies illustrates that these processes begin promptly at their thermodynamic threshold.

B. Reactions with HD

Hf^+ reacts with HD to yield both HfH^+ and HfD^+ in reactions (4) and (5) as shown in Fig. 3.

$$Hf^+ + HD \rightarrow HfH^+ + D, \quad (4)$$

$$\rightarrow HfD^+ + H. \quad (5)$$

Because of the close proximity of the product masses, there can easily be some overlap between these signals depending on the mass resolution used in the quadrupole mass filter. In the present system, it was carefully checked that high resolution leading to separation of these products could be used without sacrificing efficient collection of the product ions. The accuracy of the final results is confirmed by reasonable agreement between the magnitudes of the total cross sections for the HD system and those of the H_2 and D_2 systems (Figs. 1 and 2).

The total cross section in the HD system exhibits endothermic behavior and rises from an apparent threshold that is similar to those of the H_2 and D_2 systems. The total cross

TABLE II. Parameters of Eq. (2) used in modeling reaction (1) and its deuterated analogue and the resultant bond energies.

Reactants	Products	σ_0	n	E_0 (eV)	$D_0(Hf^+-H)$
$Hf^+ + H_2$	$HfH^+ + H$	3.5 (0.3)	0.9 (0.1)	2.42 (0.05)	2.06 (0.05)
$Hf^+ + D_2$	$HfD^+ + D$	4.0 (0.3)	1.1 (0.3)	2.34 (0.06)	2.18 (0.06)[a]

[a]Value corrected for the zero point energy difference of 0.034 eV. See text.

section reaches a maximum near the BDE of HD: 4.514 eV.[60] The individual HfH^+ and HfD^+ cross sections behave somewhat differently such that the HfD^+ cross section rises from a slightly earlier apparent onset and then peaks at a somewhat lower energy than that of HfH^+. This behavior can be rationalized because the $HfD^+ + H$ product channel has a lower energy threshold by the zero point energy difference of 0.036 eV (given the 1979 cm^{-1} vibrational frequency for HfH^+ calculated by Ohanessian *et al.*[32]). At higher energies, the HfD^+ cross section declines at an energy somewhat before the onset of dissociation in the analogue of reaction (3). The relative high-energy behavior shows that the more massive D atom carries away more energy from HfH^+ than the lighter H atom carries away from HfD^+. This effect is typical of atomic ion reactions with H_2, HD, and D_2,[4,15,18,19] and has been discussed in more detail elsewhere.[4,61–63]

C. Thermochemical results

The endothermic cross sections in the H_2 and D_2 reaction systems are analyzed in detail using Eq. (2). Typical models are shown in Figs. 1 and 2 and can be seen to reproduce the experimental results very well throughout the energy range examined. The optimum values of the parameters in Eq. (2) for these systems are listed in Table II. As can be seen in Figs. 1 and 2, the optimum values of E_0 differ appreciably from the apparent thresholds, which are largely a result of the appreciable velocity distribution of the light H_2 (D_2) reactants. Because the convoluted form of Eq. (2) includes all sources of energy (rotational, vibrational, translational, and electronic energy distributions of reactants are explicitly included in the modeling), the E_0 threshold energies determined correspond to 0 K values. From the thresholds measured, the BDEs for the metal-ligand cations observed in reaction (1) can be calculated using Eq. (6).

$$D_0(Hf^+ - H) = D_0(H_2) - E_0. \quad (6)$$

An analogous equation is used to analyze results for the deuterated system. This equation assumes that there is no activation barrier in excess of the endothermicity of the reaction, an assumption that is often true for ion-molecule reactions because of the long-range attractive forces[57] and one that can be tested using theory (see below). A summary of the Hf^+-H bond energies derived from the present experiments with both H_2 and D_2 is given in Table II. This includes adjusting the value for $D_0(Hf^+-D)$ for the zero point energy difference between HfD^+ and HfH^+. This correction uses a vibrational frequency of 1895 cm^{-1} for HfH^+ and 1344 cm^{-1} for HfD^+, as calculated here for the $^1\Sigma^+$ state (see below), a value that agrees well with a 1979 cm^{-1} value calculated by Ohanessian *et al.*[32] for HfH^+. Thus the zero point energy differences in the HfH^+ and HfD^+ bond energies are 0.034 ± 0.003 eV, assuming a 10% uncertainty in the frequencies. The Hf^+-H bond energies obtained from the H_2 and D_2 systems are in excellent agreement with one another (Table II). Our best value for this bond energy is the weighted average of these two values, 2.11 ± 0.08 eV, where the uncertainty is two standard deviations. This value is in good agreement with the value of 1.97 ± 0.11 eV for $D_0(HfH^+)$ that was previously measured in the reaction of Hf^+ with CH_4.[41] The present value is considered more reliable as there are no competing channels that might shift the threshold to higher energies.

IV. THEORETICAL CALCULATIONS

A. General

Most quantum chemistry calculations reported here are computed using the B3LYP hybrid density functional method (Becke's three-parameter exchange functional with the Lee, Yang, and Parr correlation functional)[64,65] and performed with the GAUSSIAN 03 suite of programs.[66] A large basis set is used for hydrogen, triple zeta with diffuse and polarization functions, 6-311+G(3*p*). This basis set gives good results for the thermochemistry of dihydrogen, with deviations from experiment of less than 0.03 eV for the bond energy of H–H (4.505 eV calculated versus 4.478 eV experimental).[67] The 60 core electrons of hafnium are described by the relativistic effective core potentials (ECPs) of Hay–Wadt (HW),[68] with valence electrons described by the Los Alamos double zeta basis set (LANL2DZ). This basis set is optimized for neutral atoms, whereas the positive charge differentially contracts the *s* orbitals compared to the *d* orbitals. Hence, all calculations were performed with an altered HW-ECP basis for Hf^+ as described by Ohanessian *et al.* (HW+).[32] In all cases, the thermochemistry calculated and cited here is corrected for zero point energy effects, after scaling the frequencies by 0.9804.[69] We also examined results (geometries and single point energies) calculated using Def2TZVPP, a balanced basis set of triple zeta valence quality for both elements,[70] as well as the Stuttgart–Dresden (SDD) basis set[71] for Hf [retaining the 6-311+G(3*p*) basis on hydrogen]. The Def2TZVPP basis set includes *f* and *g* type polarization functions on Hf, whereas neither the HW+ nor the SDD basis sets do. Both the Def2TZVPP and SDD basis sets use ECPs developed by Andrae *et al.*[71] for Hf.

Holthausen *et al.*[72] carefully considered the most appropriate choice for a level of theory for the first and third-row transition metal methyl cations, species analogous to the metal hydride cations considered here, because both have single covalent metal-ligand bonds. These authors used

TABLE III. Theoretical geometries and energies for HfH^+. (Results of B3LYP/HW+/6-311+G(3*p*) and B3LYP/Def2TZVPP (in italics) calculations. Energies for H at these levels of theory are −0.502 257 (*−0.498 545*) E_h).

					This work			Literature[a]		
Species	State	$s(s+1)$[b]	Configuration	Energy (E_h)	r ($M-X$) (Å)	ν (cm^{-1})[c]	E_{rel} (eV)[d]	r ($M-X$) (Å)	ν (cm^{-1})	E_{rel} (eV)
HfH^+	$^3\Delta$	2.00	$\sigma_b^2\sigma^1\delta^1$	−49.103 328	1.786	1806	0.000	1.786	1979	0.000
				−48.233 427	*1.798*	*1822*	*0.000*			
	$^1\Sigma^+$	0.00	$\sigma_b^2\sigma^2$	−49.098 748	1.747	1895	0.130			
				−48.227 966	*1.758*	*1908*	*0.154*			
	$^3\Pi$	2.00	$\sigma_b^2\sigma^1\pi^1$	−49.087 363	1.777	1784	0.433	1.779	1898	0.494
				−48.217 994	*1.789*	*1795*	*0.418*			
	$^1\Pi$	1.01	$\sigma_b^2\sigma^1\pi^1$	−49.083 655	1.781	1763	0.533			
	$^1\Delta$	1.00	$\sigma_b^2\sigma^1\delta^1$	−49.081 523	1.787	1797	0.593			
	$^3\Phi$	2.00	$\sigma_b^2\pi^1\delta^1$	−49.062 292	1.826	1674	1.108	1.829	2220	1.006
	$^3\Sigma^-$	2.00	$\sigma_b^2\delta^2$	−49.051 891	1.824	1668	1.389	1.831	1775	1.101
	$^1\Phi$	1.00	$\sigma_b^2\pi^1\delta^1$	−49.050 365	1.822	1689	1.434			
	$^1\Gamma$	0.00	$\sigma_b^2\delta^2$	−49.032 709	1.825	1721	1.916			
	$^1\Delta$	0.00	$\sigma_b^2\pi^2$	−49.009 065	1.815	1376	2.556			

[a]GVB values from Ohanessian *et al.* (Ref. 31).
[b]*s* is the spin quantum number, 0 for a singlet state, and 1 for a triplet state. Spin contamination is evident for the $^1\Pi$, $^1\Delta$, and $^1\Phi$ states.
[c]Vibrational frequencies scaled by 0.9804.
[d]Energies relative to the ground state including zero point energies.

B3LYP, Becke-half-and-half-LYP (BHLYP), and QCISD(T) (quadratic configuration interaction with single and double excitations added perturbatively) methods with a basis set consisting of a polarized double-ζ on C and H and the Hay/Wadt relativistic ECP with valence electrons added. The symmetries of the metal methyl species were constrained to C_{3v}. Upon comparison with experimental results for the first-row MCH_3^+ species (M=Sc–Cu),[29,30] these authors conclude that the B3LYP functional overbinds, whereas the BHLYP functional and the QCISD(T) methods perform more accurately. Mean absolute deviations from experiment were 0.41, 0.18, and 0.20 eV, respectively. Likewise, the bond energies calculated using B3LYP were higher than those for BHLYP and QCISD(T) for the third-row metal methyl cations. Given these results, we also performed calculations for the HfH^+ species using QCISD(T), the BHLYP functional, and CCSD(T) (coupled cluster with single and double excitations and triple excitations added perturbatively) levels of theory with the HW+, Def2TZVPP, and SDD (Ref. 71) ECPs for Hf^+. Such calculations will be explicitly noted and unless otherwise designated, our results will refer to a B3LYP/HW+/6-311+G(3*p*) level of theory. For HfH_2^+ species where multiple bonds to Hf^+ are formed, only the B3LYP functional is used. This choice is rationalized on the basis of the results of Holthausen *et al.*[73] for metal-methylene cations and our own studies of $HfCH_x^+$ (x=0–2) species.[41]

One means of evaluating the level of theory and basis set used in the calculations is to compare electronic excitation energies with those from experiment. Experimental values for the excitation energies (average over all spin-orbit states) from the ^{2}D ($6s^25d^1$) ground state to quartet states having $6s^15d^2$ and $6s^05d^3$ electron configurations are 0.563 and 2.434 eV, respectively (Table I).[54] Detailed results from various calculations are provided in supplementary material (table SI).[74] At the B3LYP and BHLYP levels of theory, similar values are obtained with excitation energies of 0.243–0.324 and 1.954–2.132 eV, slightly lower than experiment. Likewise, the values calculated at the QCISD(T) and CCSD(T) levels are nearly identical with values of 0.774–0.877 and 3.015–3.153 eV with the HW+ and SDD basis sets, somewhat higher than experiment. QCISD(T) and CCSD(T) calculations using the Def2TZVPP basis set provide the best reproduction of the experimental values: 0.508 and 2.490 eV. Thus, all levels of theory considered here reproduce the atomic excitation energies reasonably well although the QCISD(T) and CCSD(T) results are in the best agreement with experiment and the Def2TZVPP basis set performs better than the HW+/6-311+G(3*p*) combination, which is better than SDD/6-311+G(3*p*).

The experimental BDEs refer to the ground spin-orbit state at 0.0 eV, $^2D_{3/2}$ for Hf^+. In contrast, our calculations are referenced to the statistically weighted mean of all spin-orbit levels in the ground term, 0.227 eV for Hf^+ (^{2}D).[54] Because our calculations do not explicitly include spin-orbit interactions, it is possible that all calculated bond energies may need to be corrected by this different asymptotic energy before comparison with experimental values. In the generalized valence bond (GVB) calculations of Ohanessian *et al.*[32] it is suggested that spin-orbit energies may need to be taken into account in order to properly compare with experimental results. Explicit spin-orbit calculations for HfH^+ are beyond the scope of the present study.

B. HfH^+ states

The ground state of HfH^+ has been previously calculated by Ohanessian *et al.*[32] to be a $^3\Delta$ state where the character of the bonding orbital on Hf is 35% 6*s* and 64% 5*d*. The resultant bonding can be thought of as originating from a covalent sigma bond (σ_b^2) between the 1*s* orbital on H and a 6*s*5*d* hybrid orbital on Hf^+, which is formed by a combination of

TABLE IV. Bond energies (eV) calculated for the two lowest lying states of HfH^+ at several levels of theory including zero point energies.

State	Basis set	B3LYP	BHLYP	QCISD(T)	CCSD(T)
$^3\Delta$[a]	HW+[b]	**2.71, 2.59**[c] (2.09)	**2.59, 2.48**[c] (1.97)	2.34, 2.08[c] (2.06)	2.28, 2.02[c] (2.00)
	Def2[d]	**2.62, 2.62**[c] (2.17)	**2.54, 2.54**[c] (2.02)	2.39, 2.34[c] (2.05)	2.39, 2.34[c] (2.05)
	SDD[e]	**2.63, 2.63**[c] (2.11)	**2.54, 2. 54**[c] (1.99)	2.27, 2.16[c] (2.24)	2.13, 2.01[c] (2.09)
$^1\Sigma^+$[f]	HW+[b]	2.58, 2.43[c] (**2.20**)	2.42, 2.28[c] (**2.05**)	**2.74, 2.40**[c] (**2.17**)	**2.71, 2.37**[c] (**2.14**)
	Def2[d]	2.47, 2.47[c] (**2.24**)	2.31, 2.31[c] (**2.08**)	**2.61, 2.55**[c] (**2.32**)	**2.61, 2.55**[c] (**2.32**)
	SDD[e]	2.45, 2.44[c] (**2.21**)	2.30, 2.28[c] (**2.05**)	**2.79, 2.58**[c] (**2.35**)	**2.79, 2.58**[c] (**2.35**)

[a]Values in parentheses include counterpoise corrections and correspond to the adiabatic bond energy after referencing the calculation to the $Hf^+(^4F)$ asymptote and adjusting by the experimental excitation energy for this state, 0.790 eV. See text and Table I.
[b]Calculated using HW+/6-311+G(3*p*) basis set. Ground state in bold.
[c]Bond energy including counterpoise correction for basis set superposition error.
[d]Calculated using Def2TZVPP basis set for all atoms. Ground state in bold.
[e]Calculated using SDD/6-311+G(3*p*) basis set. Ground state in bold.
[f]Values in parentheses include counterpoise corrections and have been corrected by the 0.227 eV excitation for the average spin-orbit levels of the ^{2}D state. See text and Table I.

the ^{2}D ($6s^25d^1$) and ^{4}F ($6s^15d^2$) states of Hf^+. This type of hybridization is quite efficient in the third-row transition metals because relativistic effects make the 6*s* orbital comparable in size to the 5*d* orbitals. This 6*s*5*d* hybrid bonding orbital overlaps better with the 1*s* orbital on H(^{2}S) than pure 6*s* or 5*d* orbitals, even though binding to the hybrid orbital of Hf^+ requires both promotion and the loss of exchange energy because the ^{4}F state configuration is mixed in. The occupied nonbonding orbitals in the $^3\Delta$ state are $\sigma^1\delta^1$, where the σ orbital is the other 6*s*5*d* hybrid, the δ orbital is pure 5*d*, and for other states, there is a π orbital that is also pure 5*d*. The bond length calculated by Ohanessian *et al.*[32] is 1.786 Å, which is the same as the bond length calculated here at the B3LYP/HW+/6-311+G(3*p*) level.

A low-lying excited state of HfH^+ is the $^1\Sigma^+$ ($\sigma_b^2\sigma^2$) state, which lies 0.13–0.18 eV above the $^3\Delta$ ground state at the B3LYP level of theory (where the range comes from using all three basis sets noted above). The $^1\Sigma^+$ state is sufficiently close in energy to the $^3\Delta$ state that there is the possibility that this is the true ground state. The $^1\Sigma^+$ state is relatively low in energy because it can be formed directly from the Hf^+ (^{2}D, $6s^25d^1$) state (thereby avoiding promotion and exchange energy costs) by coupling the H(1*s*) electron with the $5d\sigma$ electron on Hf^+. The BHLYP level of theory agrees that the $^3\Delta$ state is the ground state, with excitation energies for the $^1\Sigma^+$ state of 0.17–0.24 eV. However, at the QCISD(T) and CCSD(T) levels of theory, the $^1\Sigma^+$ is calculated to be the ground state with the $^3\Delta$ state lying 0.22–0.52 and 0.22–0.66 eV higher, respectively (Table IV). Complicating the assignment of the true ground state is the fact that whereas the $^1\Sigma^+$ state can be derived from pure Hf^+ (^{2}D), the $^3\Delta$ state mixes in Hf^+ (^{4}F) character such that errors in the excitation energy of this state (see above and table SI) may propagate to the relative energies of the $^3\Delta$ and $^1\Sigma^+$ states. Indeed if the errors in the ^{4}F excitation energies noted above are included in full (yielding the BDEs listed in parentheses in Table IV), the $^1\Sigma^+$ state becomes the ground state at all levels of theory, with $^3\Delta$ excitation energies of 0.07–0.11, 0.06–0.08, 0.11–0.27, and 0.14–0.27 eV for the B3LYP, BHLYP, QCISD(T), and CCSD(T) calculations, respectively (Table IV). Another complication in determining the true ground state is that spin-orbit interactions will split the $^3\Delta$ state (but not the $^1\Sigma^+$), lowering the energy of one of its components, although by less than the atomic spin-orbit splitting of 0.227 eV.

We also calculated results for other stable excited states at the B3LYP/HW+/6-311+G(3*p*) level with relative energies listed in Table III. Ohanessian *et al.*[32] examined triplet excited states (but no singlet states) finding the $^3\Pi$ ($\sigma_b^2\sigma^1\pi^1$) at 0.49 eV, a $^3\Phi(\sigma_b^2\pi^1\delta^1)$ at 1.01 eV, and the $^3\Sigma^-(\sigma_b^2\delta^2)$ at 1.10 eV, all with bond lengths and excitation energies comparable to the present calculations (Table III). We located several additional singlet states, $^1\Pi$, $^1\Delta$, $^1\Phi$, $^1\Gamma$, and $^1\Delta$ with excitation energies between 0.5 and 2.6 eV (Table III).

Ohanessian *et al.* calculated a BDE for the $^3\Delta$ state of HfH^+ of 2.38 eV using GVB theory, a value somewhat above our experimental BDE. Meyer *et al.*[75] also calculated the $^3\Delta$ state of HfH^+ using multireference configuration interaction and obtained a BDE of 2.38 eV. Theoretical BDEs for this state calculated here at all levels of theory also exceed the experimental BDE if the values are referenced to the Hf^+ (^{2}D) state. If the theoretical BDEs are instead referenced to the ^{4}F state of Hf^+ and then corrected by the experimental excitation energy of the ^{4}F state for the reasons noted above, the $^3\Delta$ is no longer the ground state (Table IV). Now, the BDEs calculated for the $^1\Sigma^+$ state should be compared to the experimental value, which is still lower for all levels of theory. One reason for the discrepancy is to realize that the calculations are referenced to the average of the spin-orbit levels of Hf^+ (^{2}D), which experimentally lies 0.227 eV above the $^2D_{3/2}$ level, the experimental ground level. Therefore, the BDEs for the $^1\Sigma^+$ state in Table IV need to be reduced by this amount, as indicated by the values in parentheses. Now, the BHLYP values agree with experiment within the uncertainties, 2.05 (HW+), 2.08 (Def2TZVPP), and 2.05 (SDD) eV compared to 2.11 ± 0.08 eV. The B3LYP values remain slightly higher than experiment even with this correction, 2.20–2.24 eV, consistent with the observations of Holthausen *et al.* for metal-ligand single bonds. QCISD(T) and CCSD(T) values, which are similar to one another, also re-

TABLE V. Theoretical geometries and energies for HfH_2^+ calculated at the B3LYP/HW+/6-311+G(3*p*) level of theory.

State (configuration)	*r* (Hf–H) (Å)	*r* (H–H) (Å)	∠HHfH (deg)	Energy (E_h)	E_{rel} (eV)	ν (cm^{-1})[a]
$^2A_1(1a_1^2 1b_2^2 2a_1^1)$	1.779	2.740	100.7	−49.716 953 9	0.000	568, 1826, 1839
$^2B_1(1a_1^2 1b_2^2 1b_1^1)$	1.795	2.859	105.6	−49.698 069 6	0.513	634, 1776, 1803
$^2A_2(1a_1^2 1b_2^2 1a_2^1)$	1.788	2.640	95.2	−49.692 780 2	0.657	638, 1772, 1805
$^2B_2(1a_1^2 1b_2^1 2a_1^2)$	2.187	0.778	20.5	−49.685 250 2	0.863	455, 876, 3742
$^2B_1(1a_1^2 1b_1^1 2a_1^2)$	2.806	0.750	15.4	−49.681 595 8	0.962	18, 38, 148
$^2A_2(1a_1^2 1a_2^1 2a_1^2)$	3.487	0.745	12.3	−49.679 797 0	1.011	7, 15, 65
$^2A_1(1a_1^2 2a_1^2 3a_1^1)$	3.479	0.746	12.3	−49.679 776 8	1.012	7, 15, 67
$^4A_2(1a_1^2 1b_1^1 1b_2^1 2a_1^1)$	2.080	0.787	21.8	−49.677 154 5	1.083	697, 1075, 3295
$^4B_2(1a_1^2 1b_2^1 2a_1^1 3a_1^1)$	2.286	0.784	17.4	−49.676 974 1	1.088	520, 930, 3630
$^4B_1(1a_1^2 1b_2^1 1a_2^1 2a_1^1)$	2.114	0.794	21.7	−49.676 151 1	1.110	656, 1077, 3476
$^4A_2(1a_1^2 1a_2^1 2a_1^1 3a_1^1)$	3.448	0.746	12.4	−49.668 539 1	1.317	160, 171, 4279
$^4B_2(1a_1^2 1b_2^1 1a_2^1 2a_1^1)$	2.171	0.784	20.8	−49.668 038 8	1.331	346, 476, 4187
$^4A_1(1a_1^2 1b_2^1 1b_1^1 1a_2^1)$	1.999	0.822	23.7	−49.635 468 5	2.217	951, 1325, 3078
$^2\Sigma(1\sigma_g^2 1\sigma_u^1 2\sigma_g^2)$	1.930	3.860	180.0	−49.626 139 7	2.471	245, 296, 1065, 1419
$^4\Delta(1\sigma_g^2 1\sigma_u^1 1\delta^1 2\sigma_g^1)$	1.947	3.895	180.0	−49.622 490 5	2.570	184, 963, 1387
$^4\Pi(1\sigma_g^2 1\sigma_u^1 1\pi^1 2\sigma_g^1)$	1.912	3.825	180.0	−49.610 443 2	2.898	108, 695, 1086, 1410
$^4\Phi(1\sigma_g^2 1\sigma_u^1 1\pi^1 1\delta^1)$	1.949	3.898	180.0	−49.586 808 4	3.541	−213, 588, 1066, 1351

[a]Vibrational frequencies scaled by 0.9804. The energy of H_2 at this level of theory is −1.180 029 6 E_h with a vibrational frequency of 4418 cm^{-1} and bond length of 0.743 Å.

main slightly high, 0.03–0.24 eV above experiment, although HW+ values are within experimental uncertainty.

C. HfH_2^+ states

The properties of stable HfH_2^+ complexes found computationally are reported in Table V. For HfH_2^+, our B3LYP/HW+/6-311+G(3*p*) calculations find an inserted $^2A_1$ ground state with a BDE of 1.08 eV relative to the $Hf^+(^2D)+H_2$ asymptote. This state has a valence electron configuration of $(1a_1)^2(1b_2)^2(2a_1)^1$, where the $1a_1$ and $1b_2$ orbitals are Hf–H bonding orbitals, and the $2a_1$ is a nonbonding orbital that is mostly d_{y2} (where the symmetry axis defines the *z* coordinate and the molecule lies in the *x*-*z* plane). Furthermore, we find $^2B_1$ and $^2A_2$ excited states lying 0.51 and 0.66 eV higher in energy, respectively. The $^2B_1$ has a $(1a_1)^2(1b_2)^2(1b_1)^1$ configuration where the $1b_1$ orbital is pure Hf($5d_{yz}$), and the $^2A_2$ state has a $(1a_1)^2(1b_2)^2(1a_2)^1$ configuration where the $1a_2$ orbital is pure Hf($5d_{xy}$). An excited $^2B_2$ state was found to lie 0.86 eV above the ground state but has long Hf–H bonds and a small ∠HHfH bond angle, indicating that it is an electrostatically bound $Hf^+(H_2)$ complex. This geometry is consistent with the $(1a_1)^2(1b_2)^1(2a_1)^2$ configuration of the $^2B_2$ state, which has only three electrons in the bonding orbitals. Likewise all bent quartet states located have similar geometries because they have at most three electrons in the bonding $1a_1$ and $1b_2$ orbitals (Table V). Additionally, one doublet and several quartet states of linear HfH_2^+ were found. All of these states can be characterized as having three electrons in the σ_g and σ_u bonding orbitals, with the remaining two electrons either in the slightly antibonding σ_g, or nonbonding π or δ orbitals. These linear species have Hf^+–H bond lengths of 1.91–1.95 Å and energies of 2.47–3.54 eV relative to the $^2A_1$ state.

The complete surfaces for the various HfH_2^+ states in C_{2v} symmetry as a function of bond angle are shown in Fig. 4. These were obtained from relaxed potential energy surface (PES) scan calculations starting at the optimized geometry of each state. Because of the C_{2v} symmetry restriction, the PESs in Fig. 4 cannot examine the HfH^++H dissociation asymptote. It seems likely that these products can be formed from the HfH_2^+ intermediates with no barriers in excess of the endothermicity for the following reasons. Both the $^1\Sigma^+$ and $^3\Delta$ states of HfH^+ can interact with $H(^2S)$ to form low-spin doublet states of HfH_2^+. Covalent coupling of a nonbonding HfH^+ ($^3\Delta$) electron with H can occur along a doublet surface, such that the surface should be attractive. For the $^1\Sigma^+$ state of HfH^+, interaction with the 1*s* orbital of H gives rise to the $^2A_1(1a_1^2 1b_2^2 2a_1^1)$ state of HfH_2^+ (recogniz-

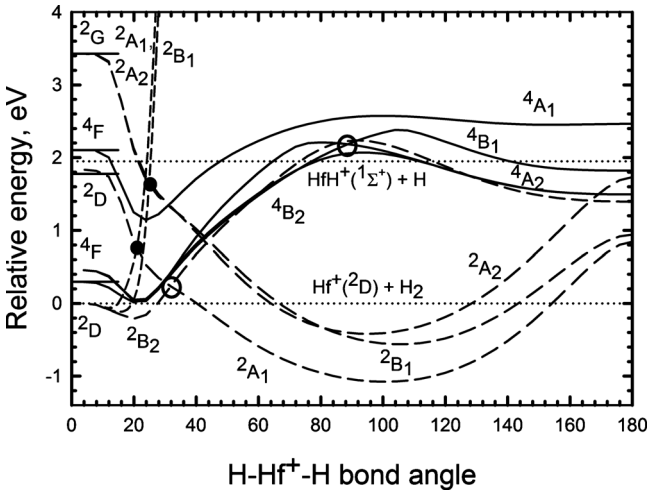

FIG. 4. B3LYP/HW+/6-311+G(3*p*) calculations of the PESs for the interaction of Hf^+ with H_2 in C_{2v} symmetry as a function of the H–Hf^+–H bond angle in degrees. Dotted lines indicate the experimental energy zero, corresponding to the $Hf^+(^2D)+H_2$ reactants at 0.0 eV, and the experimental energy of the $HfH^+(^1\Sigma^+)$+H products, 1.95 eV above the reactants. Circles indicate avoided surface crossings in C_{2v} (closed) and C_s (open) symmetry.

ing that all of these orbitals have a' symmetry as the HHf^+-H bond is broken). The $^3\Delta$ state of HfH^+ can also form high-spin quartet states of the intermediate, but these would be largely repulsive as no covalent bond formation is involved.

In Fig. 4, none of the low-lying doublet states of HfH_2^+ ($^2A_1, ^2B_1, ^2A_2$) leads diabatically to the $Hf^+(^2D, 6s^25d^1)+H_2$ reactant asymptote, but rather to $Hf^+(^2D, 6s^15d^2)$ lying 1.78 eV (2.00 eV experimental) above the ground state or $Hf^+(^2G, 5d^3)$ lying 3.43 eV (2.45 eV experimental) above the ground state. Instead, $Hf^+(^2D, 6s^25d^1)$ interacts with H_2 in C_{2v} symmetry to form four surfaces having $^2A_1$, $^2A_2$, $^2B_1$, and $^2B_2$ symmetries (another $^2A_1$ surface cannot be separately characterized). The most favorable interaction between Hf^+ and H_2 occurs when there is an acceptor orbital on the metal ion that interacts with the doubly occupied σ-bonding orbital of H_2 (having a_1 symmetry) and a donor orbital on the metal ion (the in-plane π-like orbital) that interacts with the empty σ^*-antibonding orbital of H_2 (having b_2 symmetry). Thus, the $^2B_2(1a_1^{\ 2}2a_1^{\ 2}1b_2^{\ 1})$ surface is the most attractive and leads to a well that is 0.21 eV deep with respect to the Hf^+ and H_2 reactants (at $\angle HHfH=20.5°$). When the $5d$ electron of $Hf^+(^2D)$ lies in the orbitals having b_1 (the out-of-plane π-like orbital) or a_2 (δ-like, which should also be similar to the other δ-like orbital having a_1 symmetry), much more repulsive surfaces are formed, but still lead to an $Hf^+(H_2)$ adduct with wells lying 0.12 and 0.07 eV below the reactants for $^2B_1$ and $^2A_2$, respectively. If the $5d$ electron occupies the σ-like a_1 orbital, the surface that evolves is even more repulsive. Note that this $^2A_1$ surface should have an avoided crossing with the $^2A_1$ surface evolving from the upper ^2D state of Hf^+ near 20° (as indicated by the solid circle near 0.8 eV). As the bond lengths of these two species may differ (even though the bond angles are the same), this crossing point is only suggestive, but the true crossing point is likely to be nearby. Likewise along the $^2B_1$ and $^2A_2$ surfaces, there are avoided crossings near 1.7 eV above the reactants, still below the product asymptote. Figure 4 also includes several quartet surfaces but none of these forms a particularly stable $H-Hf^+-H$ intermediate and are therefore unlikely to be important in the reactions of $Hf^+(^2D)$ with H_2.

It should be realized that C_{2v} symmetry will not occur in most reactive collisions, such that experimentally relevant surfaces will be reduced to C_s symmetry. Thus crossings between A_1 and B_2 surfaces (both A') and between B_1 and A_2 surfaces (both A'') will be avoided, as indicated by the open circles in Fig. 4. (Again these crossing points are only suggestive because the true crossing points require equal bond lengths as well.) Thus, the attractive $^2B_2(1a_1^{\ 2}1b_2^{\ 1}2a_1^{\ 2})$ surface evolving from ground state $Hf^+(^2D)+H_2$ leads to a crossing at low energies ($\sim$0.3 eV) with the $^2A_1(1a_1^{\ 2}1b_2^{\ 2}2a_1^{\ 1})$ surface leading to ground state HfH_2^+.

We also considered a collinear interaction between Hf^+ and H_2. Initial approach of $Hf^+(^2D, 6s^25d^1)$ to H_2 is attractive when the electron occupying the d orbital is in the $d\pi_{xz}$, $d\pi_{yz}$, $d\delta_{xy}$, or $d\delta_{x2-y2}$ orbital, as those orbitals do not mix with the σ orbitals of H_2. On the $^2\Pi$ surface, an Hf^+-H-H adduct is formed having a Hf–H bond length of 2.83 Å and an H–H bond length of 0.747 Å. On the $^2\Delta$ surface, the Hf^+-H-H adduct has a Hf–H bond length of 3.13 Å and a H–H bond length of 0.747 Å. Both of these surfaces have H–H bond lengths that are only slightly extended from that calculated for free H_2 of 0.743 Å. The $^2\Pi$ and $^2\Delta$ intermediates have minima lying 0.105 and 0.086 eV, respectively, below the reactant asymptote. When the d electron of $Hf^+(^2D, 6s^25d^1)$ occupies the $d\sigma_{z2}$ orbital, there is a repulsive interaction with the doubly occupied σ_g orbital of H_2. From the $^2\Pi$ and $^2\Delta$ adducts, lengthening the H–H bond leads cleanly to $^3\Pi$ and $^3\Delta$ states of HfH^+ along with $H(^2S)$, respectively.

V. DISCUSSION

A. Thermochemistry

The three group IV metal ions, Ti^+, Zr^+, and Hf^+, have MH^+ BDEs that are similar to one another: 2.31 ± 0.11, 2.26 ± 0.08, and 2.11 ± 0.08 eV, respectively.[16,19] This is unusual as third-row transition metals to the right of Hf have M^+-H BDEs that are 0.10–1.96 eV higher than their first or second-row congener. (In group III, YH^+ has a slightly higher bond energy than LaH^+.) Both Ti^+ and Zr^+ have ^4F ground states with s^1d^2 configurations and MH^+ ground states of $^3\Phi(\sigma_b^{\ 2}\pi^1\delta^1)$. In the case of Hf^+, the ground state is ^2D with a s^2d^1 configuration that leads to a $^1\Sigma^+(\sigma_b^{\ 2}\sigma^2)$, or possibly $^3\Delta(\sigma_b^{\ 2}\sigma^1\delta^1)$, ground state for HfH^+. Thus, in contrast to the lighter congeners, the stability of the s orbital relative to the d orbitals leads to preferential occupation of the nonbonding σ orbital in HfH^+. Formation of the triplet states of MH^+ involves coupling the ^4F states of M^+ with $H(^1S)$. Thus, Hf^+ needs to promote one electron in an s orbital into a d orbital to form the $^4F(6s^15d^2)$ excited state. To also include the effects of decoupling the $6s$ electron from the $5d$ electrons, we define the promotion energy as the average of the $^4F(6s^15d^2)$ and $^2F(6s^15d^2)$ excitation energies for Hf^+, yielding 1.250 eV. The ground states of Ti^+ and Zr^+ are already $^4F(s^1d^2)$ configurations, and the average of their ^4F and ^2F excitations are 0.310 and 0.429 eV, respectively. When we add these promotion energies to the BDEs of TiH^+, ZrH^+, and HfH^+, the resulting intrinsic M^+-H BDEs become 2.62, 2.69, and 3.36 eV, respectively. This comparison makes the relative MH^+ BDEs of the group IV metals comparable to the trends observed for other transition metal groups.

The $^1\Sigma^+$ state of HfH^+ is low in energy because it can be formed directly from the $^2D(6s^25d^1)$ state of Hf^+, thus avoiding promotion and exchange energy costs. However, this means that the covalent bond is formed by coupling the $1s$ electron of H with a $5d$ electron of Hf^+. As discussed previously by Ohanessian *et al.*,[32] third-row transition metal cations ordinarily form covalent bonds with H using *sd* hybrid orbitals because of the similar size of the $6s$ and $5d$ orbitals, with most species having bonding orbitals with 56%–75% d contributions (64% for the $^3\Delta$ state of Hf^+). Such hybridization is not possible for the $^1\Sigma^+$ state of HfH^+ because the $6s$ orbital on Hf^+ is already doubly occupied, such that the $^1\Sigma^+$ state has a relatively weak bond because of the poorer overlap of the $5d\sigma$ orbital of Hf^+ and the $1s$ orbital of H.

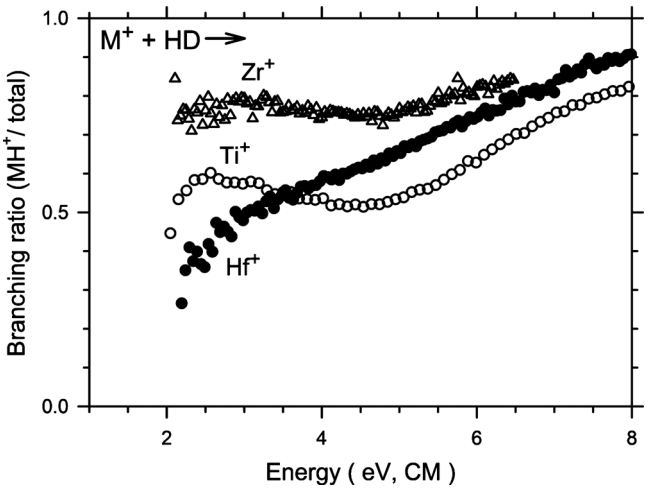

FIG. 5. Product branching fractions ($\sigma_{MH}^+/\sigma_{tot}$) for reactions of $Ti^+(^4F)$, Zr^+ (^4F), and Hf^+ (^2D) with HD as a function of kinetic energy.

B. Reaction mechanism

Further comparison of the group IV metal ions is facilitated by examining the reaction mechanisms as revealed by the reaction with HD. Previous work on the first-row and second-row transition metal cations indicates that the product branching ratio in the reaction of M^+ with HD is very sensitive to the reaction mechanism.[3,4,18,19,57] and is governed by three "rules." (1) If M^+ has an electron configuration with empty valence s and $d\sigma$ orbitals, such as for a d^n configuration where $n<5$, the reaction is efficient and may proceed by an insertion mechanism. These processes are characterized by product branching ratios in the HD system, ($\sigma_{MH}+/\sigma_{tot}$) values that are near 0.5, consistent with statistical behavior of a long-lived intermediate. (2) If either the valence s or $d\sigma$ orbital is occupied and the M^+ state is low-spin, such as for d^n ($n>5$) or low-spin coupled $d^{n-1}s^1$ configurations, the reaction occurs efficiently via a direct mechanism. These processes are characterized by a product branching ratio in the HD system that favors MH^+ by a factor of 2–4, ($\sigma_{MH}+/\sigma_{tot}$) ratios between 0.66 and 0.8, consistent with arguments concerning the conservation of angular momentum.[56,61,76–78] (3) If either the valence s or $d\sigma$ orbital is occupied and the M^+ state is high-spin (the highest spin it can possibly have), such as a high-spin coupled $d^{n-1}s^1$ configuration, the reaction is inefficient and tends to react impulsively. These processes are characterized by a product branching ratio in the HD system that favors MD^++H by a large factor, small values of the ($\sigma_{MH}^+/\sigma_{tot}$) ratio, and exhibit shifts in the thresholds for the H_2 and D_2 systems versus the HD system. Note that these rules are only appropriate for the diabatic reaction behavior, i.e., cases where the electron configuration of the metal ions remains essentially static throughout the course of the reaction.

Results for the reactions of Hf^+ are compared to those for the lighter congeners in Fig. 5 in terms of the fraction of metal hydride ion product formed. For the $^4F(s^1d^2)$ ground state configurations of both Ti^+ and Zr^+, one would expect reactions with dihydrogen according to category 3, an impulsive mechanism. For Ti^+, the data in Fig. 5 clearly indicate a statistical reaction (category 1), which was explained by the presence of a low-lying $^4F(d^3)$ state that is only 0.107 eV higher in energy.[16] This d^3 state is expected to react via a statistical mechanism and either mixes with or obscures the less reactive $Ti^+(^4F,4s^13d^2)$ ground state. For Zr^+, the data in Fig. 5 suggest reactivity between statistical and direct (category 2). This was explained by the coupling of the high-spin surfaces evolving from the ground state Zr^++H_2 reactants to those leading to the low-spin ZrH_2^+ intermediates, which would have a branching ratio that is consistent with a statistical mechanism.[19]

For $Hf^+(^2D,6s^25d^1)$, the branching ratio evolves more as a function of energy than those for Ti^+ and Zr^+. The data of Fig. 5 suggest largely statistical behavior in the region below the HD bond energy of 4.512 eV. This is consistent with the calculated PESs, which show that $Hf^+(^2D,6s^25d^1)+H_2$ reactants preferentially start off on the $^2B_2$ curve, which couples with the $^2A_1$ curve leading to a long-lived $^2A_1$ intermediate that is 1.08 eV below the reactant asymptote. This $^2A_1$ intermediate leads cleanly to the $HfH^+(^1\Sigma^+)$+H products. Other pathways couple to the $^2B_1$ and $^2A_2$ intermediates, which should also be long-lived and can form the $^3\Delta$ low-lying (or possibly ground) state.

For all three metal cations, the branching ratio above the dissociation energy of 4.5 eV increases, indicating that formation of MH^++D is favored increasingly over MD^++H. This trend is a consequence of the ability of the heavier D atom product to carry away more energy than the lighter H atom.[4,61–63]

ACKNOWLEDGMENTS

This work is supported by the National Science Foundation (Grant No. CHE-0748790).

[1] R. H. Crabtree, *The Organometallic Chemistry of the Transition Metals*, 2nd ed. (Wiley, New York, 1994).
[2] G. A. Somorjai, *Introduction to Surface Chemistry and Catalysis* (Wiley, New York, 1994).
[3] P. B. Armentrout, ACS Symp. Ser. **428**, 18 (1990).
[4] P. B. Armentrout, Int. Rev. Phys. Chem. **9**, 115 (1990).
[5] P. B. Armentrout and J. L. Beauchamp, Chem. Phys. **50**, 37 (1980).
[6] P. B. Armentrout and J. L. Beauchamp, J. Am. Chem. Soc. **103**, 784 (1981).
[7] P. B. Armentrout, L. F. Halle, and J. L. Beauchamp, J. Am. Chem. Soc. **103**, 962 (1981).
[8] P. B. Armentrout, L. F. Halle, and J. L. Beauchamp, J. Am. Chem. Soc. **103**, 6501 (1981).
[9] L. F. Halle, F. S. Klein, and J. Beauchamp, J. Am. Chem. Soc. **106**, 2543 (1984).
[10] M. L. Mandich, L. F. Halle, and J. L. Beauchamp, J. Am. Chem. Soc. **106**, 4403 (1984).
[11] M. A. Tolbert and J. L. Beauchamp, J. Am. Chem. Soc. **106**, 8117 (1984).
[12] J. L. Elkind and P. B. Armentrout, J. Chem. Phys. **84**, 4862 (1986).
[13] J. L. Elkind and P. B. Armentrout, J. Phys. Chem. **90**, 6576 (1986).
[14] J. L. Elkind and P. B. Armentrout, Inorg. Chem. **25**, 1078 (1986).
[15] J. L. Elkind and P. B. Armentrout, J. Phys. Chem. **91**, 2037 (1987).
[16] J. L. Elkind and P. B. Armentrout, Int. J. Mass Spectrom. Ion Process. **83**, 259 (1988).
[17] J. L. Elkind, L. S. Sunderlin, and P. B. Armentrout, J. Phys. Chem. **93**, 3151 (1989).
[18] Y.-M. Chen, J. L. Elkind, and P. B. Armentrout, J. Phys. Chem. **99**, 10438 (1995).
[19] M. R. Sievers, Y.-M. Chen, J. L. Elkind, and P. B. Armentrout, J. Phys. Chem. **100**, 54 (1996).
[20] X.-G. Zhang, C. Rue, S.-Y. Shin, and P. B. Armentrout, J. Chem. Phys.

116, 5574 (2002).
[21] X.-G. Zhang and P. B. Armentrout, J. Chem. Phys. **116**, 5565 (2002).
[22] F.-X. Li and P. B. Armentrout, J. Chem. Phys. **121**, 248 (2004).
[23] F.-X. Li, X.-G. Zhang, and P. B. Armentrout, J. Phys. Chem. B **109**, 8350 (2005).
[24] P. B. Armentrout, R. V. Hodges, and J. L. Beauchamp, J. Chem. Phys. **66**, 4683 (1977).
[25] P. B. Armentrout, R. V. Hodges, and J. L. Beauchamp, J. Am. Chem. Soc. **99**, 3162 (1977).
[26] P. B. Armentrout and J. L. Beauchamp, Chem. Phys. **48**, 315 (1980).
[27] R. Georgiadis and P. B. Armentrout, J. Phys. Chem. **92**, 7060 (1988).
[28] N. F. Dalleska, K. C. Crellin, and P. B. Armentrout, J. Phys. Chem. **97**, 3123 (1993).
[29] P. B. Armentrout and B. L. Kickel, in *Organometallic Ion Chemistry*, edited by B. S. Freiser (Kluwer, Dordrecht, 1996), p. 1.
[30] P. B. Armentrout, in *Topics in Organometallic Chemistry*, edited by J. M. Brown and P. Hofmann (Springer, Berlin, 1999), Vol. 4-I, p. 1.
[31] P. B. Armentrout, Int. J. Mass. Spectrom. **200**, 219 (2000).
[32] G. Ohanessian, M. J. Brusich, and W. A. Goddard III, J. Am. Chem. Soc. **112**, 7179 (1990).
[33] K. Balasubramanian and D. Dai, J. Chem. Phys. **93**, 7243 (1990).
[34] K. K. Das and K. Balasubramanian, J. Chem. Phys. **94**, 3722 (1991).
[35] D. Dai and K. Balasubramanian, J. Chem. Phys. **95**, 4284 (1991).
[36] D. Dai and K. Balasubramanian, Chem. Phys. Lett. **185**, 165 (1991).
[37] D. G. Dai, W. Cheng, and K. Balasubramanian, J. Chem. Phys. **95**, 9094 (1991).
[38] K. Balasubramanian and Z. Ma, J. Phys. Chem. **95**, 9794 (1991).
[39] H. Zhang and K. Balasubramanian, J. Phys. Chem. **96**, 6981 (1992).
[40] W. Z. Zhao, F. Buchinger, J. E. Crawford, S. Gulick, J. K. P. Lee, O. Constantinescu, M. Hussonnois, and J. Pinard, Spectrochim. Acta, Part B **51**, 707 (1996).
[41] L. G. Parke, C. S. Hinton, and P. B. Armentrout, Int. J. Mass. Spectrom. **254**, 168 (2006).
[42] S. K. Loh, D. A. Hales, L. Lian, and P. B. Armentrout, J. Chem. Phys. **90**, 5466 (1989).
[43] R. H. Schultz and P. B. Armentrout, Int. J. Mass Spectrom. Ion Process. **107**, 29 (1991).
[44] E. Teloy and D. Gerlich, Chem. Phys. **4**, 417 (1974).
[45] D. Gerlich, Adv. Chem. Phys. **82**, 1 (1992).
[46] N. R. Daly, Rev. Sci. Instrum. **31**, 264 (1960).
[47] K. M. Ervin and P. B. Armentrout, J. Chem. Phys. **83**, 166 (1985).
[48] P. J. Chantry, J. Chem. Phys. **55**, 2746 (1971).
[49] C. S. Hinton, F.-X. Li, and P. B. Armentrout, Int. J. Mass. Spectrom. **280**, 226 (2009).
[50] B. L. Kickel and P. B. Armentrout, J. Am. Chem. Soc. **117**, 4057 (1995).
[51] D. E. Clemmer, Y.-M. Chen, F. A. Khan, and P. B. Armentrout, J. Phys. Chem. **98**, 6522 (1994).
[52] C. L. Haynes and P. B. Armentrout, Organometallics **13**, 3480 (1994).
[53] B. L. Kickel and P. B. Armentrout, J. Am. Chem. Soc. **117**, 764 (1995).
[54] C. E. Moore, *Atomic Energy Levels as Derived from the Analyses of Optical Spectra*, Vol. III, NSRDS-NBS 35 (US Government Printing Office, Washington, DC, 1971).
[55] W. J. Chesnavich and M. T. Bowers, J. Phys. Chem. **83**, 900 (1979).
[56] N. Aristov and P. B. Armentrout, J. Am. Chem. Soc. **108**, 1806 (1986).
[57] P. B. Armentrout, in *Advances in Gas Phase Metal Ion Chemistry*, edited by N. G. Adams and L. M. Babcock (JAI, Greenwich, 1992), Vol. 1, p. 83.
[58] F. Muntean and P. B. Armentrout, J. Chem. Phys. **115**, 1213 (2001).
[59] M. E. Weber, J. L. Elkind, and P. B. Armentrout, J. Chem. Phys. **84**, 1521 (1986).
[60] K. P. Huber and G. Herzberg, *Molecular Spectra and Molecular Structure* (Van Nostrand Reinhold, New York, 1974), Vol. IV.
[61] J. L. Elkind and P. B. Armentrout, J. Phys. Chem. **89**, 5626 (1985).
[62] P. B. Armentrout, in *Gas Phase Inorganic Chemistry*, edited by D. H. Russell (Plenum, New York, 1989), p. 1.
[63] P. B. Armentrout, in *Selective Hydrocarbon Activation: Principles and Progress*, edited by J. A. Davies, P. L. Watson, A. Greenberg, and J. F. Liebman (VCH, New York, 1990), p. 467.
[64] A. D. Becke, J. Chem. Phys. **98**, 5648 (1993).
[65] C. Lee, W. Yang, and R. G. Parr, Phys. Rev. B **37**, 785 (1988).
[66] M. J. Frisch, G. W. Trucks, H. B. Schlegel *et al.*, GAUSSIAN 03, Revision B.02, Gaussian, Inc., Pittsburgh, PA, 2003.
[67] K. P. Huber and G. Herzberg, *Molecular Spectra and Molecular Structure* (Van Nostrand Reinhold, New York, 1979), Vol. IV.
[68] P. J. Hay and W. R. Wadt, J. Chem. Phys. **82**, 299 (1985).
[69] J. B. Foresman and Æ. Frisch, *Exploring Chemistry with Electronic Structure Methods*, 2nd ed. (Gaussian, Pittsburgh, 1996).
[70] F. Weigend and R. Ahlrichs, Phys. Chem. Chem. Phys. **7**, 3297 (2005).
[71] D. Andrae, U. Haeussermann, M. Dolg, H. Stoll, and H. Preuss, Theor. Chim. Acta **77**, 123 (1990).
[72] M. C. Holthausen, C. Heinemann, H. H. Cornehl, W. Koch, and H. Schwarz, J. Chem. Phys. **102**, 4931 (1995).
[73] M. C. Holthausen, M. Mohr, and W. Koch, Chem. Phys. Lett. **240**, 245 (1995).
[74] See supplementary material at http://dx.doi.org/10.1063/1.3482663 for one table of energies of various states of Hf^+ calculated at several levels of theory.
[75] E. R. Meyer, J. L. Bohn, and M. P. Deskevich, Phys. Rev. A **73**, 062108 (2006).
[76] L. S. Sunderlin, N. Aristov, and P. B. Armentrout, J. Am. Chem. Soc. **109**, 78 (1987).
[77] J. D. Burley, K. M. Ervin, and P. B. Armentrout, Int. J. Mass Spectrom. Ion Process. **80**, 153 (1987).
[78] P. B. Armentrout, ACS Symp. Ser. **502**, 194 (1992).